Appl. Phys. A 88, 505–518 (2007)
DOI: 10.1007/s00339-007-4043-4

Applied Physics A
Materials Science & Processing

N. BUECKING[1,2,✉]
M. SCHEFFLER[2]
P. KRATZER[3]
A. KNORR[1]

Theory of optical excitation and relaxation phenomena at semiconductor surfaces: linking density functional and density matrix theory

[1] Institut für Theoretische Physik, Nichtlineare Optik und Quantenelektronik, Technische Universität Berlin, Hardenbergstr. 36, PN 7-1, 10623 Berlin, Germany
[2] Fritz-Haber-Institut der Max-Planck-Gesellschaft, Faradayweg 4–6, 14195 Berlin, Germany
[3] Fachbereich Physik – Theoretische Physik, Universität Duisburg-Essen, Lotharstr. 1, 47048 Duisburg, Germany

Received: 6 July 2006/Accepted: 4 April 2007
Published online: 9 June 2007 •

ABSTRACT A theory for the description of optical excitation and the subsequent phonon-induced relaxation dynamics of nonequilibrium electrons at semiconductor surfaces is presented. In the first part, the fundamental dynamical equations for electronic occupations and polarisations are derived using density matrix formalism (DMT) for a surface-bulk system including the interaction of electrons with the optical field and electron–phonon interactions. The matrix elements entering these equations are either determined empirically or by density functional theory (DFT) calculations. In the subsequent parts of the paper, the dynamics at two specific semiconductor surfaces are discussed in detail. The electron relaxation dynamics underlying a time-resolved two photon photoemission experiment at an InP surface is investigated in the limit of a parabolic four band model. Moreover, the electron relaxation dynamics at a Si(100) surface is analysed. Here, the coupling parameters and the band structure are obtained from an DFT calculations.

PACS 71.15.Mb; 73.20.At; 73.43.Cd; 78.20.Bh

1 Introduction

In this work, we present a theory describing optical excitation and electron relaxation dynamics at semiconductor surfaces. It is shown how density matrix theory (DMT) can be used to derive equations of motion that include the interaction of the electrons with a radiation field and with phonons, here, within the Markov approximation. The semiconductor surface is considered as a two dimensional multi-band system containing both bulk-like and surface-like bands. To test the method, in a first approach, we restrict ourselves to four bands, and use a simple empirical ansatz for the wave functions needed to calculate matrix elements. In a second approach, we show how density functional theory (DFT) can be linked with DMT. In this context, DFT Kohn–Sham wave functions are used to calculate the electron–phonon interaction matrix elements in the dynamical equations.

The results suggest that our description is fairly realistic and that a combined approach of DMT [1–4] and DFT [5] can be successfully used to gain insight in the dynamical excitation [6] and, as shown here, relaxation processes at such surfaces.

A possible field of application for our theory are time-resolved two-photon photo-emission experiments (TR-2PPE), which have been used in numerous subfields of surface science, including image potential states [7, 8], molecules on metal surfaces [9, 10], bulk states of metals and semiconductors [11, 12] and dynamical processes combining semiconductor bulk states, surface states [13–15] and adsorbate states [16, 17]. Other theoretical descriptions are based upon optical Bloch equations [18], dynamical calculations based on Fourier grid models [19], as well as dynamical calculations for coherent pulse excitation [20, 21] and incoherent initial conditions [22, 23].

This article is organized as follows. Section 2 presents the basics of the underlying theories (DMT, DFT) as well as the calculation of the matrix elements. In Sect. 4, the application of the dynamical equations to a simple empirical model for a InP semiconductor surface is discussed. Finally, in Sect. 5, the full theory using both DFT and DMT is presented together with an application to the silicon(100) surface.

2 General approach

By performing experiments with ultrashort laser pulses, one can probe the dynamics of electrons in a solid or near its surface on the time scale of some tens of femtoseconds. On such short time-scales, coherent evolution of excited states of the systems can be observed in some cases, as long as only few distinct channels for energy dissipation are available. After the coherent time scale, relaxation processes destroy phase coherence and yield to a formation of quasi-equilibrium electron distribution functions. On the other hand, the photons in a laser pulse of 15 fs half-width are associated with an energy uncertainty of 0.1 eV. This energy scale is sufficiently small such that specific features of the electronic structure of the surface investigated are still noticeable. While the coherent and subsequent relaxation dynamics of the system calls for a description in terms of DMT, the still rather well-defined excitation energies allow for a description in terms of a quasi-particle band structure. Determination of the latter first requires a self-consistent electronic structure calculation

✉ Fax: +493031421130, E-mail: buecking@itp.physik.tu-berlin.de

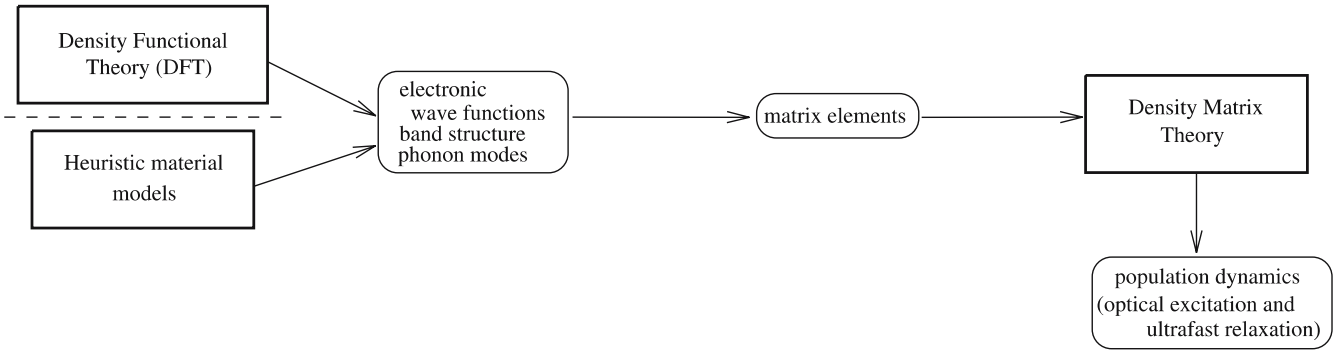

FIGURE 1 The principal structure of this approach

as starting point for calculations of the quasi-particle band structure by more elaborate methods.

While it is in principle conceivable to describe the dynamics of excited states by a single-step theory in the spirit of ab initio theories, e.g., by time-dependent DFT, such an approach is computationally cumbersome and presently still has to rely on a number of uncontrolled approximations. As an alternative, we propose a two-step approach (Fig. 1), where the relevant degrees of freedom of the dynamics are described within DMT, while the information about the microscopic processes (entering as parameters into the DMT equations) are provided by DFT. The dynamical equations for the ultra-fast response of the solid derived from density matrix theory are valid for a general multi-band system with arbitrary phonon modes. The specific system under study and its materials properties are then introduced by specifying the open parameters (matrix elements and single particle energies). This rather general setting allows us to be flexible in the modelling of the dynamics, either by retaining only a small number of bands and fixing the few remaining parameters empirically, or by working with a rather elaborate description of the electronic quasi-particle band structure and the phonon modes as delivered by ab initio methods.

DFT is capable of providing a realistic description of the surface atomic structure. However, for the excited states, the methods of many-particle perturbation theory (i.e., the GW approximation for single quasi-particle states and solutions of the Bethe–Salpeter equation for two-particle states [24]) are widely used. These methods can also be incorporated in the DMT equations via the electron–electron interaction of optically excited states [6]. Nevertheless, in this paper, we restrict ourselves to DFT calculations for the wave functions and matrix elements for electron–phonon interaction. This is acceptable as a lowest-order approximation to the actual quasi-particle wave functions and commonly used. It yields a much more detailed description and improved understanding compared to hitherto used empirical models.

2.1 *Geometry*

Compared to the bulk, a semiconductor surface system induces a symmetry reduction in the direction perpendicular to the surface. Parallel to the surface, a lattice periodicity can obviously be assumed, whereas in perpendicular direction, the bulk lattice periodicity is broken by the surface. The missing periodicity makes it inevitable to introduce a reference depth of the system, which refers to the number of layers of bulk material that are considered below surface. This configuration is called slab geometry [25–29], the slab is the reference volume of the semiconductor considered (cmp. Fig. 2). The symmetry group of the surface is determined by the reconstruction symmetry. It can be said that the slab unit cell in reciprocal space is always contained in the irreducible bulk cell [25, 26, 30].

Similarly to the restricted periodicity in real space, the first Brillouin zone of the slab is reduced to two dimensions. This means that the dispersion of the Bloch-wave functions appears only in direction parallel to the surface. The component of the bulk Bloch vector perpendicular to the surface is projected onto the two-dimensional surface Brillouin zone. Hence the number of bands per atom in the unit cell is increased in a slab calculation such that the total number of Bloch states remains the same as one would have in a bulk calculation.

2.1.1 Single particle electronic wave functions. As spin–orbit coupling is neglected and the different spin states are not treated separately in these calculations (this is well justified for silicon and a first approach for InP), the electronic states of the system are determined by two quantum numbers: a band index n and a (two dimensional) vector in reciprocal space $\underline{k} = (k_x, k_y)^{\mathrm{T}}$ (In general, in this paper, the underlined vector $\underline{v}$ will refer to a two dimensional vector in a plane parallel to surface, while the bold vector $\boldsymbol{v}$ refers to a three dimensional

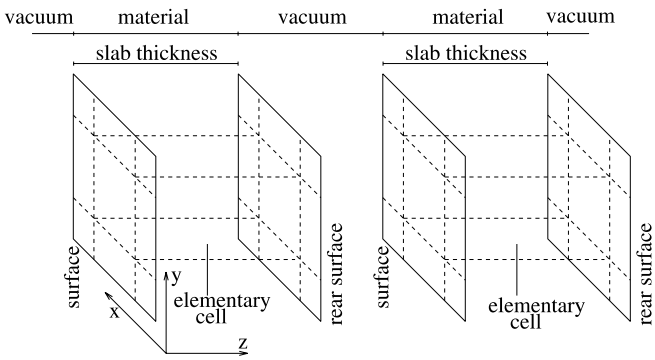

FIGURE 2 Illustration of the periodic slab model. In x and y direction, the normal lattice periodicity applies. In z-direction, periodicity is also imposed, but the vacuum layer between the slabs separates the electronic states in the different layers

vector, thus $\underline{v}$ refers to the first two components of $\boldsymbol{v}$). The result is a general form for the wave functions that is similar to the three dimensional case [25]

$$\psi_{n\underline{k}}(\boldsymbol{r}) = \frac{1}{\sqrt{\Omega_{\text{slab}}}} \mathrm{e}^{\mathrm{i}\boldsymbol{k}\boldsymbol{r}} u_{n\underline{k}}(\boldsymbol{r}) \,, \tag{1}$$

where $\boldsymbol{k} = (k_x, k_y, 0)^{\mathrm{T}}$ and Ω_{slab} is the volume of the slab. The Bloch waves $u_{n\underline{k}}(\boldsymbol{r})$ are the lattice periodic part of the wave functions with the property

$$u_{n\underline{k}}(\boldsymbol{r}+\boldsymbol{R}) = u_{n\underline{k}}(\boldsymbol{r}) \,, \tag{2}$$

for a lattice vector $\boldsymbol{R} = (R_x, R_y, 0)^{\mathrm{T}}$. The Bloch waves can be calculated by DFT or determined by a heuristic ansatz [23]. It is convenient to describe these Bloch wave functions within their Fourier representation in reciprocal space:

$$u_{n\underline{k}}(\boldsymbol{r}) = \frac{1}{\sqrt{2\pi}} \sum_{\underline{G}} u_{n\underline{k}}(\underline{G}, r_z) \, \mathrm{e}^{\mathrm{i}\underline{G}\underline{r}} \,. \tag{3}$$

Here $\{\underline{G}\}$ is the set of all reciprocal lattice vectors. If we furthermore assume that the slab is repeated periodically (Fig. 2) in the perpendicular direction with a certain amount of vacuum space between the different slabs to assure that the overlap between wave functions of neighboring slabs is negligible (which also assures that the Brillouin zone remains two-dimensional), also the third dimension of the Bloch wave can be described as a Fourier series:

$$u_{n\underline{k}}(\boldsymbol{r}) = \frac{1}{\sqrt{2\pi}} \sum_{\boldsymbol{G}} u_{n\underline{k}}(\boldsymbol{G}) \, \mathrm{e}^{\mathrm{i}\boldsymbol{G}\boldsymbol{r}} \,, \tag{4}$$

with a now three dimensional set of lattice vectors $\{\boldsymbol{G}\}$. This frequently allows a simpler evaluation of matrix elements such as momentum matrix elements for electron–light coupling.

2.1.2 Phonon modes. As for the electronic wave functions in Sect. 2.1.1, similar considerations apply to the phonon modes of a slab. While parallel to surface, the movement of the atoms at the coordinates $\boldsymbol{X}_j = (\underline{X}_j, z_j)^{\mathrm{T}} = (x_j, y_j, z_j)^{\mathrm{T}}$ can be described by an exponential

$$\boldsymbol{s}_{\underline{q}}(\boldsymbol{X}_j, t) = \sum_i \boldsymbol{s}_{i\underline{q}}(z_j) \, \mathrm{e}^{\mathrm{i}(\underline{q}\underline{X}_j - \omega_{i\underline{q}} t)} \,, \tag{5}$$

where i counts the normal modes. The dependence of $\boldsymbol{s}_{i\underline{q}}$ on (z_j) reflects the change of the bulk modes due to the surface and the surface reconstruction. In this work, a simpler approach is used. We approximate $\boldsymbol{s}_{i\underline{q}}(z_j)$ by the corresponding bulk modes, such that:

$$\boldsymbol{s}_{\underline{q}}(\boldsymbol{X}_j, t) = \sum_l \boldsymbol{s}_{l\boldsymbol{q}} \, \mathrm{e}^{\mathrm{i}(\boldsymbol{q}\boldsymbol{X}_j - \omega_{l\underline{q}} t)} \,, \tag{6}$$

By this ansatz, the surface modes are neglected. Note that in this case, q_z appears as a new parameter in the overall mode count index. The bulk modes in slab geometry can be derived from the modes in a typical irreducible bulk structure (e.g., diamond structure), so the phonon dispersion (and also the deformation potentials in Sect. 3.1) can be obtained either from bulk calculations or from experimental bulk data without using surface properties.

2.2 *Density matrix formalism*

In second quantization, all observables, like the total electron density $\varrho(\boldsymbol{r}) = \sum_{n\underline{k},n'\underline{k}'} \psi^*_{n\underline{k}}(\boldsymbol{r}) \psi_{n'\underline{k}'}(\boldsymbol{r}) \langle a^\dagger_{n\underline{k}} a_{n'\underline{k}'} \rangle$ and macroscopic polarization density $\mathcal{P}(t) = \sum_{n\underline{k},n'\underline{k}'} d_{n\underline{k},n'\underline{k}'} \langle a^\dagger_{n\underline{k}} a_{n'\underline{k}'} \rangle$, are expressed in terms of creation ($a^\dagger_{n\underline{k}}$) and annihilation operators ($a_{n'\underline{k}'}$) [2, 31]. In a system containing electrons and phonons, we define the electronic operators $a^\dagger_{n\underline{k}}$ and $a_{n\underline{k}}$ with the fermionic commutation relation

$$\left[a^\dagger_{n\underline{k}}, a_{n'\underline{k}'} \right]_+ = \delta_{n,n'} \delta_{\underline{k},\underline{k}'} \tag{7a}$$

and the phonon operators $b^\dagger_{i,\underline{q}}$ and $b_{i,\underline{q}}$ with the bosonic commutation relation

$$\left[b^\dagger_{i\underline{q}}, b_{i'\underline{q}'} \right]_- = \delta_{i,i'} \delta_{\underline{q},\underline{q}'} \,. \tag{7b}$$

The introduced quantum numbers of the operators correspond to the quantum numbers of the electron wave functions and phonon modes (Sect. 2.1). The preparation of a quantum system can be expressed in terms of the density operator. The expectation value of an arbitrary operator O is then given by

$$\langle O(t) \rangle = \mathrm{tr}(\varrho O(t)) \,. \tag{8}$$

For the investigation of the ultrafast population dynamics, the observables to be looked at dynamically are the expectation values of number operators

$$f_{n\underline{k}} = \left\langle a^\dagger_{n\underline{k}} a_{n\underline{k}} \right\rangle \,, \tag{9a}$$

for electrons (describing the probability to find an electron in state $\psi_{n\underline{k}}(\boldsymbol{r})$),

$$n_{i\underline{q}} = \left\langle b^\dagger_{i\underline{q}} b_{i,\underline{q}} \right\rangle \,, \tag{9b}$$

for phonons (describing to the probability to find a phonon in the mode i at wavevector $\underline{q}$) and the electronic polarizations (transition probability amplitudes)

$$p_{\substack{n\underline{k} \\ n'\underline{k}'}} = \left\langle a^\dagger_{n\underline{k}} a_{n'\underline{k}'} \right\rangle \,, \tag{9c}$$

which describe the transitions (or coherence) between the states. The considered system Hamiltonian in second quantization consists of four parts:

$$\begin{aligned} \mathcal{H} = & \underbrace{\sum_{n\underline{k}} E_{n\underline{k}} a^\dagger_{n\underline{k}} a_{n\underline{k}}}_{\text{I}} + \underbrace{\sum_{i\underline{q}} \hbar\omega_{i\underline{q}} b^\dagger_{i\underline{q}} b_{i\underline{q}}}_{\text{II}} \\ & + \underbrace{\sum_{\substack{n\underline{k} \\ n'\underline{k}'}} \boldsymbol{A}(t) \boldsymbol{p}_{\substack{n\underline{k} \\ n'\underline{k}'}} a^\dagger_{n\underline{k}} a_{n'\underline{k}'}}_{\text{III}} \\ & + \underbrace{\sum_{\substack{n\underline{k} \\ n'\underline{k}' \\ i\underline{q}}} D_{\substack{n\underline{k} \\ n'\underline{k}' \\ i\underline{q}}} a^\dagger_{n\underline{k}} a_{n'\underline{k}'} (b^\dagger_{i-\underline{q}} + b_{i\underline{q}})}_{\text{IV}} \,. \end{aligned} \tag{10}$$

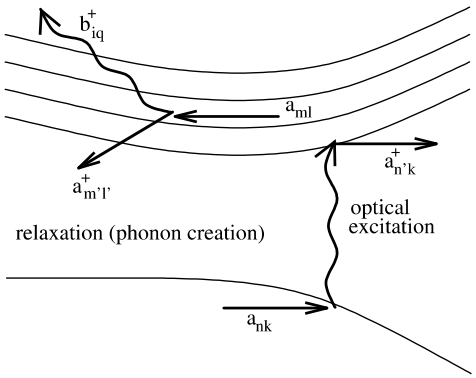

FIGURE 3 Illustration of the processes treated by our theory. After optical excitation, electrons are redistributed within the conduction bands $a_{m'l'} \rightarrow a^{\dagger}_{m'\underline{l}'}$ by emission $b^{\dagger}_{iq}$ or absorption b_{iq} of phonons

Part I contains the kinetic energy of the electrons with the energy of the single particle electron states $E_{n\underline{k}}$, part II the phonon energy with the phonon dispersion relation $\omega_{i\underline{q}}$. Part III describes coupling to the electromagnetic vector potential $\boldsymbol{A}(t)$ with the momentum matrix element $\boldsymbol{p}_{n\underline{k},n'\underline{k}'}$ within dipole approximation [32]. Part IV contains the electron–phonon coupling with the coupling element $D_{n\underline{k},n'\underline{k}',i\underline{q}}$, cmp. Fig. 3. $E_{n\underline{k}}$ and $\omega_{i\underline{q}}$ represent the equilibrium properties of the system before the optical excitation where electrons and phonons are decoupled. The calculation of the momentum matrix element and the electron–phonon coupling elements will be discussed in Sect. 3.

2.3 *Equations of motion*

2.3.1 General form. To derive equations for the dynamics of operators, Heisenberg's equation of motion can be used [2, 33]

$$\mathrm{i}\hbar\frac{\mathrm{d}}{\mathrm{d}t}O = [O, \mathcal{H}]. \tag{11}$$

Inserting the electronic polarization operators $a^{\dagger}_{m\underline{l}}a_{m'\underline{l}'}$ into (11) [4, 34], we obtain a non-closed hierarchy of equations, as illustrated in the following:

$$\begin{aligned}
\mathrm{i}\hbar\frac{\mathrm{d}}{\mathrm{d}t}(a^{\dagger}_{m\underline{l}}a_{m'\underline{l}'}) &= \left[a^{\dagger}_{m\underline{l}}a_{m'\underline{l}'}, \mathcal{H}\right] \\
&= \left(E_{m\underline{l}} - E_{m'\underline{l}'}\right) a^{\dagger}_{m\underline{l}}a_{m'\underline{l}'} \\
&\quad + \boldsymbol{A}(t)\sum_{n\underline{k}}\left(\boldsymbol{p}_{\substack{m\underline{l}\\ n\underline{k}}}a^{\dagger}_{n\underline{k}}a_{m'\underline{l}'} - \boldsymbol{p}_{\substack{n\underline{k}\\ m'\underline{l}'}}a^{\dagger}_{m\underline{l}}a_{n\underline{k}}\right) \\
&\quad + \sum_{n\underline{k}}\left(D_{\substack{m\underline{l}\\ n\underline{k}\\ i\underline{q}}}a^{\dagger}_{n\underline{k}}a_{m'\underline{l}'}\left(b^{\dagger}_{i,-\underline{q}} + b_{i,\underline{q}}\right)\right. \\
&\quad \left. - D_{\substack{n\underline{k}\\ m'\underline{l}'\\ i\underline{q}}}a^{\dagger}_{m\underline{l}}a_{n\underline{k}}\left(b^{\dagger}_{i,-\underline{q}} + b_{i,\underline{q}}\right)\right).
\end{aligned} \tag{12a}$$

A close look on these equations shows that these equations for the polarization operators $a^{\dagger}_{m\underline{l}}a_{m'\underline{l}'}$ depend on the dynamics of three operator products like $a^{\dagger}_{m\underline{l}}a_{n\underline{k}}b^{\dagger}_{i\underline{q}}$. The equations of motion for those quantities that can be derived using (11):

$$\begin{aligned}
\mathrm{i}\hbar\frac{\mathrm{d}}{\mathrm{d}t}(a^{\dagger}_{m\underline{l}}a_{m'\underline{l}'}b^{\dagger}_{i,-\underline{q}}) &= \left(E_{m\underline{l}} - E_{m'\underline{l}'} + \hbar\omega_{i\underline{q}}\right) a^{\dagger}_{m\underline{l}}a_{m'\underline{l}'}b^{\dagger}_{i,-\underline{q}} \\
&\quad + \boldsymbol{A}(t)\sum_{n\underline{k}}\left(\boldsymbol{p}_{\substack{m\underline{l}\\ n\underline{k}}}a^{\dagger}_{n\underline{k}}a_{m'\underline{l}'}b^{\dagger}_{i,-\underline{q}} - \boldsymbol{p}_{\substack{n\underline{k}\\ m'\underline{l}'}}a^{\dagger}_{m\underline{l}}a_{n\underline{k}}b^{\dagger}_{i,-\underline{q}}\right) \\
&\quad + \sum_{\substack{n\underline{k}\\ i'\underline{q}'}} D_{\substack{m\underline{l}\\ n\underline{k}\\ i'\underline{q}'}}a^{\dagger}_{n\underline{k}'}a_{m'\underline{l}'}\left(b^{\dagger}_{i',-\underline{q}'}b^{\dagger}_{i,-\underline{q}} + b_{i'\underline{q}'}b^{\dagger}_{i,-\underline{q}}\right) \\
&\quad - \sum_{\substack{n\underline{k}\\ i'\underline{q}'}} D_{\substack{n\underline{k}\\ m'\underline{l}'\\ i'\underline{q}'}}a^{\dagger}_{m\underline{l}}a_{n\underline{k}}\left(b^{\dagger}_{i',-\underline{q}'}b^{\dagger}_{i,-\underline{q}} + b_{i'\underline{q}'}b^{\dagger}_{i,-\underline{q}}\right) \\
&\quad + \sum_{\substack{n\underline{k}\\ n'\underline{k}'}} D_{\substack{n\underline{k}\\ n'\underline{k}'\\ i\underline{q}}}a^{\dagger}_{m\underline{l}}a_{m'\underline{l}'}a^{\dagger}_{n\underline{k}}a_{n'\underline{k}'}
\end{aligned} \tag{12b}$$

and similarly for the adjoint operator products.

From (12) it can be recognized that the resulting equations couple now to products of four operators. The corresponding dynamical equations for the four operator terms depend on even higher order contributions. Consequently, at this point, there is no alternative to approximations that truncate or close the hierarchy of terms in these differential equations. Sections 2.3.2 – 2.3.4 summarize a set of approximations to close the hierarchy of the equations of motion.

2.3.2 Correlation expansion. The method of choice to break this hierarchy is a generalized mean field approach for higher order correlations called correlation expansion [35–37]. This method has been used for several applications [4, 34, 36, 38, 39]. The principal idea is to approximate the expectation value of an arbitrary N-order operator $\langle a^{\dagger}_{n_1\underline{k}_1}\ldots a^{\dagger}_{n_r\underline{k}_r} a_{m_1\underline{k}_1}\ldots\ a_{m_s\underline{k}_s}\ b^{\dagger}_{i_1\underline{q}_1}\ldots b^{\dagger}_{i_t\underline{q}_t}\ b_{j_1\underline{w}_1}\ldots b_{j_u\underline{w}_u}\rangle$ where $N = r + s + t + u$ by a combination of the expectation values up to an arbitrary order $M \leq N$ of all possible correlations of the operators from the original expectation value. The sign of the correlation terms of order M is determined by the commutation relations supplied for the single operators. With the generation scheme for the dynamical equations introduced above (the order of the operators is increased by one with every new step), the maximum order of the expectation values that figure inside the equations is $M+1$ for an order of M considered. Due to the fact that electron conservation is assumed for the whole system, only those expectation values don't vanish that contain an equal number of electronic creation and annihilation operators $r = s$.

2.3.3 Bath hypothesis. For typical excitation conditions in surface experiments, it is reasonable to assume that the phonon distribution remains always close to thermal equilibrium, as the temperature is fairly elevated and weak coupling is assumed [35]. Consequently, the phonons will be assumed to stay in an equilibrium state and the expectation value of phononic operators can only be non-vanishing

if creation and annihilation operators combine to thermal equilibrium distribution for a bosonic system, given by the *Bose-distribution*:

$$\left\langle b^{\dagger}_{i\underline{q}} b_{i\underline{q}} \right\rangle = n_{i\underline{q}}(T) \frac{1}{\mathrm{e}^{\frac{\hbar\omega_{i\underline{q}}}{k_{\mathrm{B}}T}} - 1}, \tag{13}$$

where T is the temperature of the system, k_{B} the Boltzmann constant and $\hbar\omega_{i\underline{q}}$ the phonon energy dispersion. On this level of approximation, the equations of motion (12) can be simplified and the hierarchy of equations can be closed. The resulting equations are given by

$$\begin{aligned}
\mathrm{i}\hbar \frac{\mathrm{d}}{\mathrm{d}t} p_{\substack{m\underline{l} \\ m'\underline{l}'}} &= \left(E_{m\underline{l}} - E_{m'\underline{l}'}\right) p_{\substack{m\underline{l} \\ m'\underline{l}'}} \\
&\quad + \boldsymbol{A}(t) \sum_{n\underline{k}} \left(\boldsymbol{p}_{\substack{m\underline{l} \\ n\underline{k}}} p_{\substack{n\underline{k} \\ m'\underline{l}'}} - \boldsymbol{p}_{\substack{n\underline{k} \\ m'\underline{l}'}} p_{\substack{m\underline{l} \\ n\underline{k}}} \right) \\
&\quad + \sum_{\substack{n\underline{k} \\ i\underline{q}}} \left(D_{\substack{m\underline{l} \\ n\underline{k} \\ i\underline{q}}} \left\langle a^{\dagger}_{n\underline{k}} a_{m'\underline{l}'} b^{\dagger}_{i,-\underline{q}} \right\rangle + D_{\substack{m\underline{l} \\ n\underline{k} \\ i\underline{q}}} \left\langle a^{\dagger}_{n\underline{k}} a_{m'\underline{l}'} b_{i\underline{q}} \right\rangle \right. \\
&\quad \left. - D_{\substack{n\underline{k} \\ m'\underline{l}' \\ i\underline{q}}} \left\langle a^{\dagger}_{m\underline{l}} a_{n\underline{k}} b^{\dagger}_{i,-\underline{q}} \right\rangle - D_{\substack{n\underline{k} \\ m'\underline{l}' \\ i\underline{q}}} \left\langle a^{\dagger}_{m\underline{l}} a_{n\underline{k}} b_{i\underline{q}} \right\rangle \right)
\end{aligned} \tag{14a}$$

and

$$\begin{aligned}
\mathrm{i}\hbar \frac{\mathrm{d}}{\mathrm{d}t} \left\langle a^{\dagger}_{m\underline{l}} a_{m'\underline{l}'} b^{\dagger}_{i,-\underline{q}} \right\rangle &= \left(E_{m\underline{l}} - E_{m'\underline{l}'} + \hbar\omega_{i\underline{q}}\right) \left\langle a^{\dagger}_{m\underline{l}} a_{m'\underline{l}'} b^{\dagger}_{i,-\underline{q}} \right\rangle \\
&\quad + \boldsymbol{A}(t) \sum_{n\underline{k}} \left(\boldsymbol{p}_{\substack{m\underline{l} \\ n\underline{k}}} \left\langle a^{\dagger}_{n\underline{k}} a_{m'\underline{l}'} b^{\dagger}_{i,-\underline{q}} \right\rangle - \boldsymbol{p}_{\substack{n\underline{k} \\ m'\underline{l}'}} \left\langle a^{\dagger}_{m\underline{l}} a_{n\underline{k}} b^{\dagger}_{i,-\underline{q}} \right\rangle \right) \\
&\quad + \sum_{n\underline{k}} \left(D_{\substack{m\underline{l} \\ n\underline{k} \\ i\underline{q}}} p_{\substack{n\underline{k} \\ m'\underline{l}'}} n_{i\underline{q}}(T) - D_{\substack{n\underline{k} \\ m'\underline{l}' \\ i\underline{q}}} p_{\substack{m\underline{l} \\ n\underline{k}}} \left(n_{i\underline{q}}(T) + 1\right) \right) \\
&\quad + \sum_{\substack{n\underline{k} \\ n'\underline{k}'}} D_{\substack{n\underline{k} \\ n'\underline{k}' \\ i\underline{q}}} p_{\substack{m\underline{l} \\ n'\underline{k}'}} p_{\substack{n\underline{k} \\ m'\underline{l}'}} .
\end{aligned} \tag{14b}$$

This system of differential equations can in principle be solved to obtain the electron distribution dynamics (9a), by an adequate solving algorithm like a Runge–Kutta method. Nevertheless the numerical effort is considerable, as it represents a set of approximately $N^2 \times K^3$ coupled equations, where N is the number of bands and K the number of $\underline{k}$-points. On the other hand, a further approximation can reduce the numerical effort considerably. It is well known that in weakly coupled systems with a set of dense electronic states within the energy range of interest, where scattering partners are easily available, does not depend strongly on the dynamics of the phonon assisted density matrices. This is a converse behaviour as found in quantum dots where only discrete energy levels with a level separation well above the phonon energy are involved [1, 4, 40]. Thus, a major simplification of the equations can be achieved by applying a Markovian approximation to the dynamics.

2.3.4 Markov approximation. The Markov approximation is an adiabatic elimination of the dynamics of the phonon-assisted density matrices (14b) from that of ordinary density matrices (14a) [34]. Neglecting the optical interaction in perturbation theory ($\boldsymbol{A}(t) = 0$), (14b) can be integrated formally:

$$\begin{aligned}
\left\langle a^{\dagger}_{m\underline{l}} a_{m'\underline{l}'} b^{\dagger}_{i,-\underline{q}} \right\rangle &= \frac{\mathrm{i}}{\hbar} \int_0^{\infty} \mathrm{e}^{\frac{\mathrm{i}}{\hbar}\left(E_{m\underline{l}} - E_{m'\underline{l}'} - \hbar\omega_{i\underline{q}}\right)t'} \mathrm{d}t' \\
&\quad \times \left(\sum_{n\underline{k}} D_{\substack{m\underline{l} \\ n\underline{k} \\ i\underline{q}}} n_{i\underline{q}}(T)\, p_{\substack{n\underline{k} \\ m'\underline{l}'}}(t - t') \right. \\
&\quad - \sum_{n\underline{k}} D_{\substack{n\underline{k} \\ m'\underline{l}' \\ i\underline{q}}} \left(n_{i\underline{q}}(T) + 1\right) p_{\substack{m\underline{l} \\ n\underline{k}}}(t - t') \\
&\quad \left. + \sum_{\substack{n\underline{k} \\ n'\underline{k}'}} D_{\substack{n\underline{k} \\ n'\underline{k}' \\ i\underline{q}}} p_{\substack{m\underline{l} \\ n'\underline{k}'}}(t - t') p_{\substack{n\underline{k} \\ m'\underline{l}'}}(t - t') \right) .
\end{aligned} \tag{15}$$

If the dynamics of the electron polarizations $p_{m\underline{l},m'\underline{l}'}$ inside the integral of the formal solution of (15) is assumed to be dominated by the free propagation:

$$p^{\mathrm{free}}_{\substack{m\underline{l} \\ m'\underline{l}'}}(t - t') = \mathrm{e}^{-\frac{\mathrm{i}}{\hbar}\left(E_{m\underline{l}} - E_{m'\underline{l}'}\right)t'} p_{\substack{m\underline{l} \\ m'\underline{l}'}}(t) , \tag{16}$$

the integral in (15) can be solved and the phonon-assisted density matrices can be eliminated in (14a). Consequently, a new set of equations is found, which depends now only on the equal-time terms of the polarizations. If this is finally reinserted into (14a), the third order operator terms are totally disposed of and we find the following equations for the polarizations:

$$\begin{aligned}
\mathrm{i}\hbar \frac{\mathrm{d}}{\mathrm{d}t} p_{\substack{m\underline{l} \\ m'\underline{l}'}} &= \left(E_{m\underline{l}} - E_{m'\underline{l}'}\right) p_{\substack{m\underline{l} \\ m'\underline{l}'}} \\
&\quad + \boldsymbol{A}(t) \sum_{n\underline{k}} \left(\boldsymbol{p}_{\substack{m\underline{l} \\ n\underline{k}}} p_{\substack{n\underline{k} \\ m'\underline{l}'}} - \boldsymbol{p}_{\substack{n\underline{k} \\ m'\underline{l}'}} p_{\substack{m\underline{l} \\ n\underline{k}}} \right) \\
&\quad - \frac{\mathrm{i}}{\hbar} \sum_{\substack{n\underline{k} \\ n'\underline{k}' \\ n''\underline{k}'' \\ i\underline{q}}} D_{\substack{n\underline{k} \\ m'\underline{l}' \\ i\underline{q}}} D_{\substack{n'\underline{k}' \\ n''\underline{k}'' \\ i\underline{q}}} \left(\Delta\left(E_{n'\underline{k}'} - E_{n\underline{k}} - \hbar\omega_{i\underline{q}}\right) \right. \\
&\quad \times \left(\left(n_{i\underline{q}} + 1\right) p_{\substack{m\underline{l} \\ n'\underline{k}'}} \left(\delta_{n,n''} \delta_{\underline{k},\underline{k}''} - p_{\substack{n\underline{k} \\ n''\underline{k}''}} \right) \right. \\
&\quad \left. - n_{i\underline{q}} \left(\delta_{m,n'} \delta_{\underline{l},\underline{k}'} - p_{\substack{m\underline{l} \\ n'\underline{k}'}} \right) p_{\substack{n\underline{k} \\ n''\underline{k}''}} \right) \\
&\quad + \Delta\left(E_{n'\underline{k}'} - E_{n\underline{k}} + \hbar\omega_{i\underline{q}}\right) \\
&\quad \times \left(n_{i\underline{q}} p_{\substack{m\underline{l} \\ n'\underline{k}'}} \left(\delta_{n,n''} \delta_{\underline{k},\underline{k}''} - p_{\substack{n\underline{k} \\ n''\underline{k}''}} \right) \right. \\
&\quad \left. \left. - \left(n_{i\underline{q}} + 1\right) \left(\delta_{m,n'} \delta_{\underline{l},\underline{k}'} - p_{\substack{m\underline{l} \\ n'\underline{k}'}} \right) p_{\substack{n\underline{k} \\ n''\underline{k}''}} \right) \right)
\end{aligned}$$

$$
\begin{aligned}
&-\frac{\mathrm{i}}{\hbar}\sum_{\substack{n\underline{k}\\ n'\underline{k}'\\ n''\underline{k}''\\ i\underline{q}}} D_{\substack{m\underline{l}\\ n\underline{k}\\ i\underline{q}}} D_{\substack{n''\underline{k}''\\ n'\underline{k}'\\ i\underline{q}}} \left(\Delta^*\left(E_{n'\underline{k}'}-E_{n\underline{k}}-\hbar\omega_{i\underline{q}}\right)\right.\\
&\times\left((n_{i\underline{q}}+1)\,p_{\substack{m'\underline{l}'\\ n'\underline{k}'}}\left(\delta_{n'',n}\delta_{\underline{k}'',\underline{k}}-p_{\substack{n''\underline{k}''\\ n\underline{k}}}\right)\right.\\
&-n_{i\underline{q}}\left(\delta_{m',n'}\delta_{\underline{l}',\underline{k}'}-p_{\substack{m'\underline{l}'\\ n'\underline{k}'}}\right)p_{\substack{n''\underline{k}''\\ n\underline{k}}}\Bigg)\\
&+\Delta^*\left(E_{n'\underline{k}'}-E_{n\underline{k}}+\hbar\omega_{i\underline{q}}\right)\\
&\times\left(n_{i\underline{q}}\,p_{\substack{n'\underline{k}'\\ m'\underline{l}'}}\left(\delta_{n'',n}\delta_{\underline{k}'',\underline{k}}-p_{\substack{n''\underline{k}''\\ n\underline{k}}}\right)\right.\\
&\left.\left.-(n_{i\underline{q}}+1)\left(\delta_{n',m'}\delta_{\underline{k}',\underline{l}'}-p_{\substack{n'\underline{k}'\\ m'\underline{l}'}}\right)p_{\substack{n''\underline{k}''\\ n\underline{k}}}\right)\right)\Bigg),
\end{aligned}
\tag{17}
$$

where the "half space delta" $\Delta(\omega)$ is defined as $\Delta(\omega)=\int_0^\infty \mathrm{e}^{\mathrm{i}\omega t}\,\mathrm{d}t$. Two further simplifications are applied to this system of equations. First, the polaron shift is neglected by setting $\Delta(\omega)=\pi\delta(\omega)$. Second, the phonon scattering is restricted to diagonal terms by imposing $m=n'$, $n=n''$, $\underline{l}=\underline{k}'$ and $\underline{k}=\underline{k}''$. This is justified, as the dependence on the polarizations $p_{n\underline{k},n'\underline{k}'}$ is typically a higher order effect. The resulting equations for the electron coherences and the occupations are of a much simpler general form:

$$
\begin{aligned}
\mathrm{i}\hbar\frac{\mathrm{d}}{\mathrm{d}t}p_{\substack{m\underline{l}\\ m'\underline{l}'}} &= \left(E_{m\underline{l}}-E_{m'\underline{l}'}\right)p_{\substack{m\underline{l}\\ m'\underline{l}'}}\\
&\quad+\boldsymbol{A}(t)\sum_{n\underline{k}}\left(\boldsymbol{p}_{\substack{m\underline{l}\\ n\underline{k}}}p_{\substack{n\underline{k}\\ m'\underline{l}'}}-\boldsymbol{p}_{\substack{n\underline{k}\\ m'\underline{l}'}}p_{\substack{m\underline{l}\\ n\underline{k}}}\right)\\
&\quad-\left(\Gamma^{\mathrm{in}}_{m\underline{l}}+\Gamma^{\mathrm{out}}_{m\underline{l}}+\Gamma^{\mathrm{in}}_{m'\underline{l}'}+\Gamma^{\mathrm{out}}_{m'\underline{l}'}\right)p_{\substack{m\underline{l}\\ m'\underline{l}'}}
\end{aligned}
\tag{18a}
$$

$$
\begin{aligned}
\mathrm{i}\hbar\frac{\mathrm{d}}{\mathrm{d}t}f_{m\underline{l}} &= \boldsymbol{A}(t)\sum_{n}\left(\boldsymbol{p}_{\substack{m\underline{l}\\ n\underline{k}}}p_{\substack{n\underline{k}\\ m\underline{l}}}-\boldsymbol{p}_{\substack{n\underline{k}\\ m\underline{l}}}p_{\substack{m\underline{l}\\ n\underline{k}}}\right)\\
&\quad+2\Gamma^{\mathrm{in}}_{m\underline{l}}\left(1-f_{m\underline{l}}\right)-2\Gamma^{\mathrm{out}}_{m\underline{l}}f_{m\underline{l}}\,.
\end{aligned}
\tag{18b}
$$

The scattering rates are then given by

$$
\begin{aligned}
\Gamma^{\mathrm{in}}_{m\underline{l}} &= \frac{\mathrm{i}}{\hbar}\sum_{\substack{n\underline{k}\\ i\underline{q}}}\left|D_{\substack{m\underline{l}\\ n\underline{k}\\ i\underline{q}}}\right|\left(\delta\left(E_{m\underline{l}}-E_{n\underline{k}}-\hbar\omega_{i\underline{q}}\right)\right.\\
&\quad\times\left(\left(n_{i\underline{q}}+1\right)f_{m\underline{l}}-n_{i\underline{q}}\left(1-f_{m\underline{l}}\right)\right)\\
&\quad+\delta\left(E_{m\underline{l}}-E_{n\underline{k}}+\hbar\omega_{i\underline{q}}\right)\\
&\quad\times\left.\left(n_{i\underline{q}}f_{m\underline{l}}-\left(n_{i\underline{q}}+1\right)\left(1-f_{m\underline{l}}\right)\right)\right)
\end{aligned}
\tag{19a}
$$

and

$$
\begin{aligned}
\Gamma^{\mathrm{out}}_{m\underline{l}} &= \frac{\mathrm{i}}{\hbar}\sum_{\substack{n\underline{k}\\ i\underline{q}}}\left|D_{\substack{m\underline{l}\\ n\underline{k}\\ i\underline{q}}}\right|\delta\left(\left(E_{m\underline{l}}-E_{n\underline{k}}-\hbar\omega_{i\underline{q}}\right)\right.\\
&\quad\times\left(\left(n_{i\underline{q}}+1\right)f_{m\underline{l}}-n_{i\underline{q}}\left(1-f_{m\underline{l}}\right)\right)\\
&\quad+\delta\left(E_{n'\underline{k}'}-E_{n\underline{k}}+\hbar\omega_{i\underline{q}}\right)\\
&\quad\times\left.\left(n_{i\underline{q}}f_{m\underline{l}}-\left(n_{i\underline{q}}+1\right)\left(1-f_{m\underline{l}}\right)\right)\right)\,.
\end{aligned}
\tag{19b}
$$

The physical meaning of these equations is obvious. For instance, the rhs of (18) consists of two contributions. The first counts the scattering processes into the state $m\underline{l}$ (which depends on the probability, that this state is not occupied, e.g., $1-f_{m\underline{l}}$, the other one counts the scattering processes out of this state, this depends on the probability that the state is occupied $f_{m\underline{l}}$. Inside the scattering rates (19), it can be seen that only energy conserving scattering events are possible with these assumptions and scattering is highly influenced by the phonon distribution and thus depends highly on temperature.

If no optical excitation is considered, only the electron distribution and not the polarization of these equations have to be taken, leading to a numerically much simpler set of equations [1, 2, 4, 41]:

$$
\mathrm{i}\hbar\frac{\mathrm{d}}{\mathrm{d}t}f_{m\underline{l}}=2\Gamma^{\mathrm{in}}_{m\underline{l}}\left(1-f_{m\underline{l}}\right)-2\Gamma^{\mathrm{out}}_{m\underline{l}}f_{m\underline{l}}\,.
\tag{20}
$$

3 Matrix elements and interaction parameters

Within the second quantization procedure, the coupling contributions beyond the equilibrium state are given by two contributions: First, there is the electron light coupling (term III in (10)), its strength given by the momentum matrix (25). Second, there is electron–phonon coupling where the corresponding matrix elements involve single-particle electronic and phononic states.

3.1 *Electron–phonon coupling and matrix elements*

The electron–phonon interaction Hamiltonian incorporates part IV of the Hamiltonian (10). Generally, the coupling parameters $D_{n\underline{k},n'\underline{k}',i\underline{q}}$ are composed of a $\underline{q}$-dependent factor that has to be specified according to the material system, and a matrix element overlap from the electron states involved in the corresponding scattering process. $D_{n\underline{k},n'\underline{k}',i\underline{q}}$ is given by the Fourier transform of the electron–phonon interaction potential [31, 42, 43]. In the deformation potential approximation, only the first term in the Fourier series is taken into account (the potential is assumed to be slowly varying within the semiconductor). Taking as further assumption the bulk-projected phonon modes from (6), one can derive a simplified general form for the matrix elements:

$$
D_{\substack{n\underline{k}\\ n'\underline{k}'\\ i\underline{q}}}=D_{i\underline{q}}\int_{\mathbb{R}^3}\mathrm{d}r^3\,\psi_{n\underline{k}}(\boldsymbol{r})^*\,\mathrm{e}^{\mathrm{i}\underline{q}\underline{r}}\psi_{n'\underline{k}'}(\boldsymbol{r})\,.
\tag{21}
$$

Within these assumptions, the general form of the coupling parameters is given by

$$
D_{i\underline{q}}\,\mathrm{e}^{\mathrm{i}\underline{q}\underline{r}}\sqrt{\frac{\hbar}{2\varrho V\omega_{i\underline{q}}}}\,V\underbrace{\frac{\partial E}{\partial V}}_{\mathrm{I}}\underbrace{\frac{\Delta V}{V}}_{\mathrm{II}}\Bigg|_{i\underline{q}},
\tag{22}
$$

where part I refers to the energy variation ∂E by a relative volume change ∂V and part II describes the relative change of the volume induced by the dynamical evolution of the of the phonon modes, for example for LA-phonons we have $\Delta V/V = \nabla \boldsymbol{s}(\boldsymbol{r}, t)$, where $\boldsymbol{s}(\boldsymbol{r}, t)$ is the longitudinal elongation field, ϱ the material density and $\omega_{i\underline{q}}$ the phonon dispersion [43]. In general, also coupling to transversial modes can be described in this manner. This is called the deformation potential approach. Furthermore, the alternative form for the Bloch waves (4) produces the following result:

$$\begin{aligned} D_{\substack{n\underline{k} \\ n'\underline{k}' \\ i\underline{q}}} &= D_{i\underline{q}} \frac{1}{2\pi} \sum_{\boldsymbol{G},\boldsymbol{G}'} u^*_{n\underline{k}}(\boldsymbol{G}) u_{n'\underline{k}'}(\boldsymbol{G}') \\ &\quad \times \int_{\mathbb{R}^3} \mathrm{d}r^3 \, \mathrm{e}^{-\mathrm{i}(\boldsymbol{k}+\boldsymbol{G})\boldsymbol{r}} \, \mathrm{e}^{\mathrm{i}\boldsymbol{q}\boldsymbol{r}} \, \mathrm{e}^{\mathrm{i}(\boldsymbol{k}'+\boldsymbol{G}')\boldsymbol{r}} \\ &= D_{i\underline{q}} \frac{1}{2\pi} \sum_{\boldsymbol{G},\boldsymbol{G}'} u^*_{n\underline{k}}(\boldsymbol{G}) u_{n'\underline{k}'}(\boldsymbol{G}') \delta_{\boldsymbol{G}'+\boldsymbol{k}'+\boldsymbol{q},\boldsymbol{G}+\boldsymbol{k}} \,. \end{aligned} \tag{23}$$

The δ-condition in (23) allows two conclusions. First, there exists an elementary symmetry (hermiticity) relation for the coupling constants where

$$D_{\substack{n\underline{k} \\ n'\underline{k}' \\ i\underline{q}}} = D^*_{\substack{n'\underline{k}' \\ n\underline{k} \\ i,-\underline{q}}} \,. \tag{24}$$

This identity can help to reduce the computational effort. Second, there is the possibility of scattering processes over the boundaries of the Brillouin zone, if $\underline{k}' + \underline{q} > \underline{G}$. In the simulations, this cannot be neglected. In the limiting case that $\underline{k}, \underline{k}'$ and $\underline{q}$ are small with respect to the lattice vectors, the known property of momentum conservation for scattering processes is fulfilled with $\underline{k} = \underline{k}' + \underline{q}$, e.g., scattering is only possible, if the $\underline{k}$-vector of the initial electron state and the $\underline{q}$-vector of the phonon mode match the $\underline{k}$-vector of the final electron state.

The coupling mechanism $D_{i\underline{q}}$ of electrons and phonons depends strongly on the material system considered [43]. While for a polar semiconductor, Fröhlich coupling dominates the interaction, for non-polar materials no prevailing coupling mechanism can be identified. The deformation potential approximation (22) can be employed either with parameters $D_{i\underline{q}}$ from experiment or from ab initio calculations [44, 45] or by applying other coupling mechanisms like Fröhlich coupling.

3.2 *Optical matrix elements*

The electron–light coupling (term III in the Hamiltonian (10)) can be derived from $\boldsymbol{A}(t)\boldsymbol{p}_{n\underline{k},n'\underline{k}'}$ coupling, where $\boldsymbol{A}(t)$ denotes the electromagnetic vector potential within Coulomb gauge and $\boldsymbol{p}_{n\underline{k},n'\underline{k}'}$ is the single particle momentum matrix element [46]

$$\boldsymbol{p}_{\substack{n\underline{k} \\ n'\underline{k}'}} = \int_{\mathbb{R}^3} \mathrm{d}r^3 \psi_{n\underline{k}}(\boldsymbol{r})^* \frac{\hbar}{\mathrm{i}} \nabla \psi_{n'\underline{k}'}(\boldsymbol{r}) \,. \tag{25}$$

As for the electron–phonon coupling, we use (4) to examine the symmetries of these matrix elements:

$$\boldsymbol{p}_{\substack{n\underline{k} \\ n'\underline{k}'}} = \frac{1}{2\pi} \sum_{\boldsymbol{G},\boldsymbol{G}'} u^*_{n\underline{k}}(\boldsymbol{G}) u_{n'\underline{k}'}(\boldsymbol{G}') \int_{\mathbb{R}^3} \mathrm{d}r^3 \, \mathrm{e}^{-\mathrm{i}(\boldsymbol{k}+\boldsymbol{G})\boldsymbol{r}} \frac{\hbar}{\mathrm{i}} \nabla \, \mathrm{e}^{\mathrm{i}(\boldsymbol{k}'+\boldsymbol{G}')\boldsymbol{r}} \tag{26}$$

$$= \frac{1}{2\pi} \sum_{\boldsymbol{G}} u^*_{n\underline{k}}(\boldsymbol{G}) \big(\boldsymbol{G} + \boldsymbol{k}\big) u_{n'\underline{k}}(\boldsymbol{G}) \,. \tag{27}$$

Obviously, these matrix elements are diagonal in $\underline{k}$. This results from the dipole approximation and spatially homogeneous excitation of the surface [47]. Furthermore, the relation $\boldsymbol{p}_{n\underline{k},n'\underline{k}} = \boldsymbol{p}^*_{n'\underline{k},n\underline{k}}$ is exploited to reduce the numerical effort.

3.3 *Calculation of matrix elements with density functional theory (DFT)*

In the dynamics described within the DMT formalism, the quantities specifying the material enter as (so far undetermined) parameters. These parameters contain the information about the two-dimensional surface band structure and the momentum- and phonon–electron interaction matrix elements ((27) and (23)), which are derived from the unperturbed (in the sense of a Hamiltonian without electromagnetic and electron–phonon interaction) single particle states.

In the literature, various methods are in use to obtain the required information about the electronic structure. For example, a $\boldsymbol{k} \cdot \boldsymbol{p}$ expansion around the extrema of the conduction and valence bands is useful for describing the electronic structure of semiconductor nanostructures [48]. However, this method is inappropriate for surfaces [23], where scattering processes extend on the whole Brillouin zone and an accurate description of surface states is required. It appears, therefore, inevitable to use a method that can provide both an accurate description of the atomic structure, the wave functions and the band structure over a wide range on the Brillouin zone. We chose density functional theory with the LDA approximation for investigating the silicon(100) surface. Though the bandgap of the Kohn–Sham band structure differs from the experimental (optical) bandgap, the difference between the DFT-LDA exchange-correlation energy and the many-body self energy is practically independent of the $\boldsymbol{k}$-vector. We will therefore use the DFT-LDA Kohn–Sham wave functions for the evaluations of the matrix elements. A similar approach has been investigated in [6] to study coherent optical effects. In contrast, in this paper, we focus on the relaxation dynamics of non-equilibrium distributions.

Similar to the discussion of DMT, we briefly review the basic concepts of DFT. DFT is widely used to calculate the total energy of poly-atomic systems (atoms, molecules or solids). It is a first-principles approach, meaning that it only uses the chemical identity of the atoms (their nuclear charge) as input. By relaxing the atomic structures using forces that are also calculated from the first-principles electronic structure, it is possible to obtain accurate geometries of structures that are difficult to determine experimentally, in particular the atomic structure of surfaces.

DFT is an in principle exact theory built on the Hohenberg–Kohn theorem [49]. In the proof of this theorem,

it is shown that a one-to-one mapping exists between the potential entering the many-body Hamiltonian due to the atoms or ions (in this technical context called the external potential, $V(\boldsymbol{r})$) and the electron density of the system,

$$n(\boldsymbol{r}) = \sum_{i=1}^{N} \int \mathrm{d}r_1 \ldots \mathrm{d}r_N |\Psi_i(\boldsymbol{r}_1, \ldots, \boldsymbol{r}_N)|^2 \delta(r - r_i) \,. \tag{28}$$

Here, Ψ is the many-particle wavefunction. Consequently, all other quantities, in particular the many-particle wavefunction, are functionals of the electron density. Moreover, it is shown that the total energy of the system in the electronic ground state, as a functional of the density, is stationary around the true ground state density. Hence the ground state energy E_0 can be found by minimizing the energy functional

$$E[n] = \langle \Psi[n] | H | \Psi[n] \rangle \tag{29}$$

under the constraint that $\int \mathrm{d}r\, n(\boldsymbol{r})$ is preserved.

In most practical applications, DFT is employed in the special form devised by Kohn and Sham [50]. They introduce a fictitious non-interacting electron system with the same density as the physical (interacting) system of interest. In this approach, the total energy $E[n]$ is decomposed into the kinetic energy of the non-interacting system, $T_\mathrm{s}[n]$, the Hartree energy, the energy due to the external potential $V(\boldsymbol{r})$, and the exchange-correlation energy $E_\mathrm{XC}[n]$,

$$\begin{aligned} E[n] =& T_\mathrm{s}[n] + \frac{\mathrm{e}^2}{8\pi\varepsilon_0} \int\int \frac{n(\boldsymbol{r}) n(\boldsymbol{r}')}{|\boldsymbol{r} - \boldsymbol{r}'|} \mathrm{d}^3 r \, \mathrm{d}^3 r' \\ &+ \int n(\boldsymbol{r}) V(\boldsymbol{r}) \, \mathrm{d}^3 r + E_\mathrm{XC}[n] \,. \end{aligned} \tag{30}$$

The last term, E_XC, incorporates all the quantum mechanical many-particle effects beyond the Hartree approximation. By performing the variation $\delta E[n]/\delta n(\boldsymbol{r})$, a set of equations for single-particle wave functions φ_i (describing the fictitious non-interacting electron system), the Kohn–Sham equations, are obtained:

$$\varepsilon_i \varphi_i(\boldsymbol{r}) = -\frac{\hbar^2}{2m} \Delta \varphi_i(\boldsymbol{r}) + V_\mathrm{eff}(\boldsymbol{r}) \varphi_i(\boldsymbol{r}) \,. \tag{31}$$

These equations are formally similar to the single-particle Schrödinger equation with an effective potential

$$V_\mathrm{eff}(\boldsymbol{r}) = V(\boldsymbol{r}) + V_\mathrm{H} + V_\mathrm{XC}[n](\boldsymbol{r}) \,, \tag{32}$$

where the second term is the Hartree potential,

$$V_\mathrm{H}(\boldsymbol{r}) = \frac{\mathrm{e}^2}{4\pi\varepsilon_0} \int \frac{n(\boldsymbol{r}')}{|\boldsymbol{r} - \boldsymbol{r}'|} \mathrm{d}^3 r' \,, \tag{33}$$

and last term, the exchange-correlation potential, stands for $\delta E_\mathrm{XC}[n]/\delta n(\boldsymbol{r})$. Since $n(\boldsymbol{r})$ enters in the expression for V_eff, the Kohn–Sham equations (31) must be solved self-consistently with the density determined from the single-particle wave functions.

Since the exchange-correlation functional $E_\mathrm{XC}[n(\boldsymbol{r})]$ is not known analytically for the general case of a spatially varying electron density, approximative functionals must be employed. In our case, the local density approximation (LDA) is used.

While the solutions of the Kohn–Sham equations refer to a fictitious non-interacting system of electrons in an effective potential, the quantities entering the DMT formalism, as long as electron–electron interaction is not considered in the DMT Hamiltonian (10), are the quasi-particle band structure and wave functions of the elementary excitations of the system. Therefore, in general, further improvements on top of the Kohn–Sham LDA results are required. While some success in improving excitation energies has been made by using time-dependent density functional theory with suitable functionals, the established methods to account for the difference between the interacting and the Kohn–Sham system use many-particle perturbation theory (for a comparison of both approaches, see e.g. [24]). Formally, a self-energy operator Σ is introduced as the solution of Dyson's equation, and the difference between the interacting and the non-interaction system, described by $\Delta\Sigma(\boldsymbol{r}, \boldsymbol{r}', z) = \Sigma(\boldsymbol{r}, \boldsymbol{r}', z) - V_\mathrm{XC}(\boldsymbol{r}))\delta(\boldsymbol{r} - \boldsymbol{r}')$, is expanded into a perturbation series in the basis defined by the solutions of the Kohn–Sham equations:

$$E_i = \varepsilon_i + \sum_j \frac{\langle \varphi_j | \Delta\Sigma | \varphi_i \rangle}{\varepsilon_i - \varepsilon_j + i\eta} + \ldots \tag{34a}$$

$$\psi_i = \varphi_i + \sum_j \frac{\Delta\Sigma | \varphi_i \rangle}{\varepsilon_i - \varepsilon_j + i\eta} + \ldots \,. \tag{34b}$$

For the quasi-particle band structure describing single excitations, typically the GW approximation for Σ is used, and Dyson's equation is solved approximately with Fourier-space methods. In cases where $\Sigma(\boldsymbol{k}, \boldsymbol{k}', z)$ depends only weakly on $\boldsymbol{k}$ and $\boldsymbol{k}'$, (34b) describes just a rigid shift of bands. For many semiconductors, as for silicon, this is a reasonable approximation (scissors shift). In this work, we are mostly interested in matrix elements. If the use the scissors shift is justified for the band structure calculations, it is also justified to use Kohn–Sham wave functions directly to calculate the required matrix elements, as they can be considered as a first-order approximation of the quasi-particle wave functions.

We note that the combined DMT + DFT approach leaves room to add the electronic many-particle effects contained in Σ also at a later stage, in the form of Coulomb terms in the DMT-Hamiltonian. If one follows this option, double-counting should be avoided, i.e., one would prefer to work in a basis of uncorrected Kohn–Sham states (as we in fact do here). As our DFT software provides the wave functions for Bloch states in reciprocal space, the form of (23) for the matrix elements is very useful.

4 Electron relaxation and TR-2PPE dynamics at indium phosphide surfaces

In this section we illustrate the intrinsic possibilities of the proposed approach by showing how the theory can be applied to study actual experiments. The first simulations have been carried out on a highly simplified surface model with a schematic form of both the band structure and the wave functions and the resulting matrix elements[1]. This first simulation intends to describe experiments on a clean indium phosphide (100) surface [13, 22, 23]. The band structure is known

[1] The following material parameters are used: valence band min. 0 eV, conduction band min. 1.339 eV, surface band min. 1.589 eV, vacuum

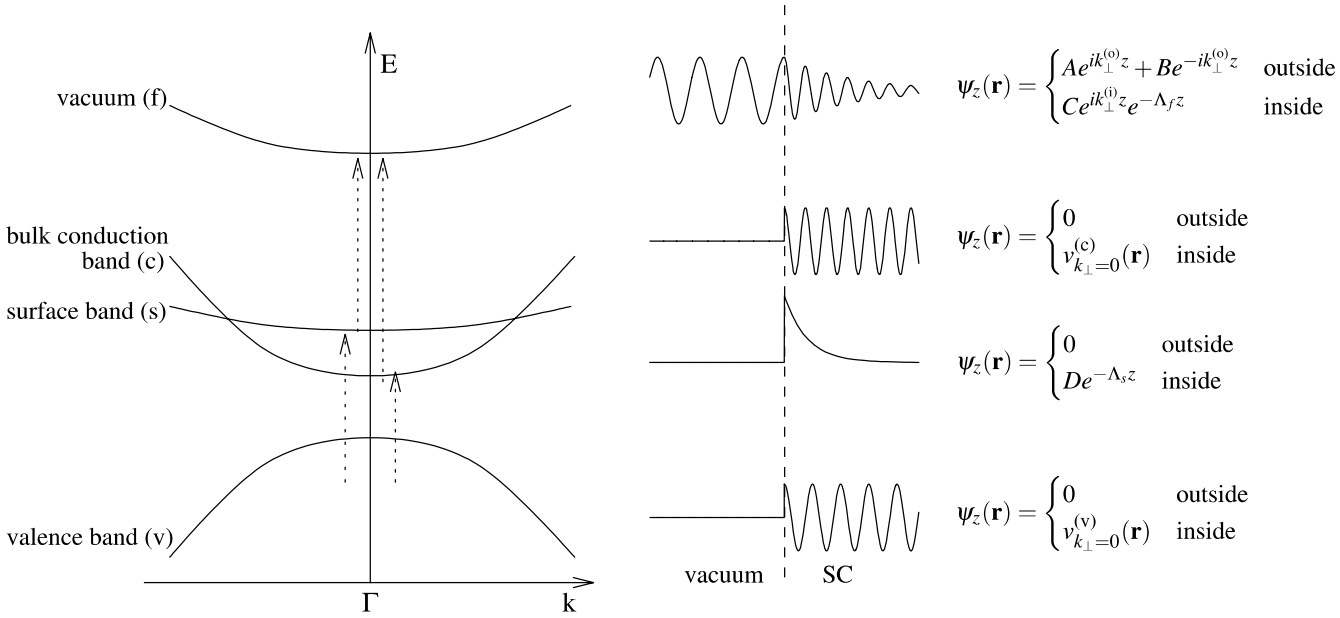

FIGURE 4 Model band structure and wave functions perpendicular to the surface used to model the InP(001) surface. The constants A, B, C, D, $k_\perp^{(i)}$ and $k_\perp^{(o)}$ are either chosen in order to assure continuity at the surface (A,B,C) or to fulfill a normalization condition of the wave function (D) (cmp. [23]). $v^{(c)}_{k_\perp=0}(\boldsymbol{r})$ and $v^{(v)}_{k_\perp=0}(\boldsymbol{r})$ are Bloch wave function at $k = \bar{\Gamma}$ taken from Bulk theory. All parameters used are given in footnote 1. The *arrows* indicate the possible optical excitation processes between these bands

to feature a surface conduction band which energetically overlaps with the bulk conduction bands [51–55] (Fig. 4). A special feature of this band system is a bulk conduction band minimum energetically below the surface conduction band minimum (cp. Fig. 4). Corresponding time resolved two photon photoemission experiments have been realised [13, 56] to study the electron transfer between bulk and surface bands. These aspects will be discussed in Sect. 4.2.

4.1 *Band structure and wave functions*

The simplified band structure (Fig. 4) is described by approximated parabolic bands [22, 23]. Four different types of bands are covered within this model: 1. A three-dimensional isotropic valence band (v). The third dimension perpendicular to surface is treated by a band-pseudo index mapping the three-dimensional $\boldsymbol{k}$-space with N sample points to our two dimensional model of Sect. 2.1 with N bands. This band populated with electrons before the optical excitation processes. 2. A three-dimensional bulk conduction band (c). The mapping to two dimensions is done similarly to the valence band case. This band, however, plays a major role in the electron–phonon dynamics, as it couples strongly to the surface band via electron–phonon scattering. 3. A two-dimensional surface conduction band (s). This band and c can be populated via electrons lifted from v. 4. The evanescent electron states (in three dimensions) for the emitted electrons in vacuum (f). These states only exist outside the semiconductor and within a small region below the surface. The parameters for this band structure are derived from experimental data[1]. To filter out the irrelevant physical processes, only a subset of the possible interaction channels are treated: optical excitation is possible from the valence band to the bulk and surface conduction bands, and from the bulk and surface conduction bands to the vacuum band. Phonon interaction is only taken into account between and inside bulk and surface conduction bands.

For each of the bands, a corresponding simplified wave function is given in [23] (Fig. 4). Within the parabolic band approximation, the Bloch wave functions of (2) are normally taken independent from the $\boldsymbol{k}$-vector throughout the whole Brillouin zone. For simplicity, we suppose an abrupt decay of the valence and conduction bulk bands at surface. Inside the semiconductor, the wave functions of bulk material at $\boldsymbol{k} = 0$ are taken.

For the surface band, an exponential decay Λ_s in the inside of the semiconductor is assumed. The reference depth $1/\Lambda_\mathrm{s}$ remains as open parameter in the simulation which has to be reasonably adjusted by a corresponding DFT calculation [22] to be $\Lambda_\mathrm{s} = 0.5\,\mathrm{nm}^{-1}$. Outside the semiconductor, the surface band states are also set to zero. The vacuum states, finally, are harmonic waves on the outside of the semiconductor an show up a decay Λ_f in the inside of the semiconductor. This decay rate also remains as a parameter in the calculations which is adjusted to $\Lambda_\mathrm{f} = 2.4\,\mathrm{nm}^{-1}$. The number of open parameters is one of the disadvantages of this empirical approach.

The main contribution to phonon–electron interaction for this InP material system is Fröhlich-coupling due to the polarity [43]. Consequently, it is a good assumption to use only one single longitudinal optical phonon mode. Its coupling strength

band min. 7.7 eV, effective masses: $m^\mathrm{v}_\mathrm{eff} = -0.45m_\mathrm{e}$, $m^\mathrm{c}_\mathrm{eff} = 0.078m_\mathrm{e}$, $m^s_\mathrm{eff} = 0.2m_\mathrm{e}$, $m^\mathrm{f}_\mathrm{eff} = 1.0m_\mathrm{e}$, surface band damping $\Lambda_\mathrm{s} = 0.5\,\mathrm{nm}^{-1}$, vacuum band penetration depth $\Lambda_\mathrm{f} = 2.4\,\mathrm{nm}^{-1}$, $\varepsilon_0 = 9.52$, $\varepsilon_\infty = 12.35$, $T = 300$ K, Phonon energy 43 meV, dipole matrix elements: val./cond. 0.3 e nm, val./surf. 1.2/0.0 e nm, cond./vac. = 0.3 e nm, surf./vac. = 0.09 e nm. See [23].

is well described by the dielectric properties of the material. Furthermore, as the dispersion of this optical mode is rather constant, it is no great loss to assume a constant energy for all phonons. With this choice of the wave functions the matrix elements for the desired processes can be calculated. Due to the simplified form of the expressions, the matrix elements can be derived analytically. The bulk–surface coupling element is given by

$$D_{\substack{\mathrm{c},k_z,\underline{k} \\ \mathrm{s}\underline{k}' \\ \mathrm{LO},q_z,\underline{q}}} = \sqrt{\frac{\mathrm{e}^2\hbar\omega_{\mathrm{LO}}}{2V\varepsilon_0\varepsilon_{\mathrm{phon}}}}\delta_{\underline{k}',\underline{k}+\underline{q}}\frac{\mathrm{i}\Lambda_{\mathrm{s}}^{\frac{1}{2}}}{q_z - k_z + \frac{\mathrm{i}\Lambda_{\mathrm{s}}}{2}}D_{\mathrm{c,s}} \tag{35}$$

where

$$D_{\mathrm{c,s}} = \int \mathrm{d}^3 r u_{\mathrm{c}}^*(\boldsymbol{r})u_{\mathrm{s}}(\boldsymbol{r}) \tag{36}$$

is the matrix element between the bulk electron states at Γ for the s and the c band. $D_{\mathrm{c,s}}$ must be smaller than 1 due to the normalization of the wave functions [22].

4.2 *Results*

In time resolved two photon photoemission (TR-2PPE) experiments a material is exposed to two short light pulses with a distinct temporal delay. The first pulse (pump pulse) is used to populate conduction band states from the valence band, the second pulse (probe pulse) performs an electron ionization and emission from the excited conduction band states, allowing a temporally resolved picture of the de-excitation processes of the excited states by varying the delay between the pulses.

In order to investigate the relaxation processes in the InP material, the optical excitation through the pump pulse and subsequent relaxation process in the conduction bands is simulated. As a realistic initial condition, a pulse of a temporal length of 40 fs located around $t = 0$ is chosen. In Fig. 5, the population of the bulk and surface conduction bands is plotted over the energy axis for variable temporal delays between the pulses ranging from 0 fs to 1000 fs. At $t = 100$ fs, when the pump pulse has finished, both surface and bulk conduction bands are populated, in the subsequent time steps, it is clearly visible that the population relaxes to the bulk band minimum.

The model calculation within the this 4 band model system shows qualitatively a very good agreement with the experimental results. In [23], theoretical results for the TR-2PPE are given. It appears probable that the proposed dynamical processes (electron relaxation through phonons) are indeed responsible for the observed processes in recent experiments [13]. Nevertheless, the simulations cannot be considered as quantitatively correct, as the phonon–electron matrix elements $D_{\mathrm{c,s}}$ (36), limited by to a maximum size of 1.0 by the normalization condition of the wave functions, had to be increased up to a value of 4.0 to obtain the experimentally observed order of magnitude for the scattering time, and the approximate solution of the evolution equation is no longer unique in this limit. It is likely that a more accurate description for the band structure and the phonon coupling is needed,

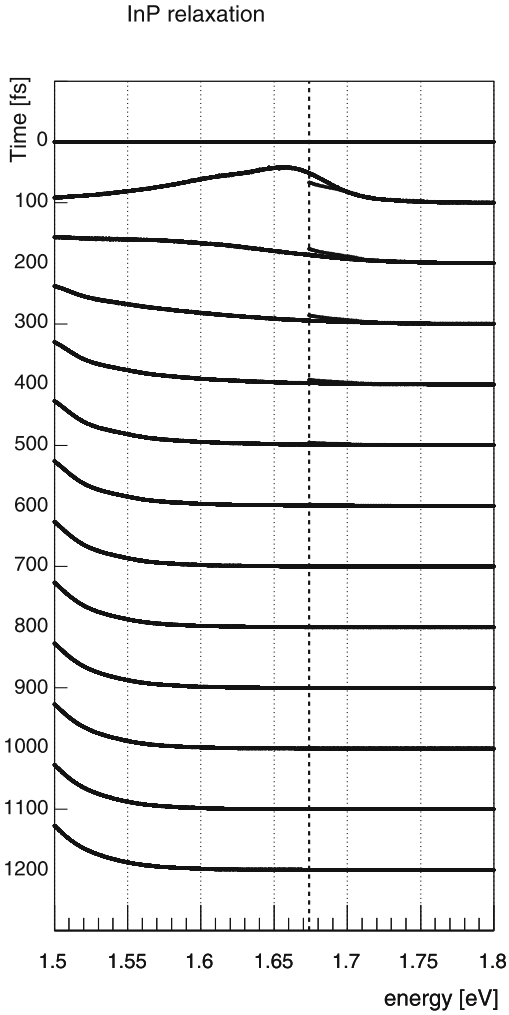

FIGURE 5 Relaxation of InP after optical excitation. The *dashed line* indicates the surface band minimum. At $t = 0$, the conduction states are unoccupied. After excitation, both states relax from an initial occupation to towards the bulk band minimum

in particular for $\boldsymbol{k}$-points distant from the Γ-point in the Brillouin zone which appear to be of a certain importance for the scattering in this material. Additionally, there is evidence that the overall size of the bulk-surface phonon–electron coupling elements are overestimated by the choice of the simple surface wave functions (Fig. 4).

5 Electron relaxation at silicon(100) surfaces

The somewhat unsatisfactory approach in Sect. 4 (basically the use of model wave functions instead of ab initio wave functions) can be made considerably more realistic by using atomic structures and the corresponding electronic wave functions from density functional theory calculations. In a first approach, we focus on the electron relaxation dynamics in an already well characterized materials system, the silicon(100) surface. In this system, a number of excitation and relaxation processes [14] have been observed on different timescales involving the D^{down} surface state. In particular, the interplay of bulk–bulk, bulk–surface and surface–surface scattering governs the dynamics of the electrons. The aim of

this work is to find a first theoretical and parameter-free description for these observations.

5.1 *Ab initio calculation of material parameters*

The calculation for this materials system should accomplish mainly two tasks: Firstly, an accurate description of the surface relaxation should be reached, as atomic displacements are known to have a high influence on the localization and nature of surface states. Secondly, the band structure and associated single electron states have to be found, which are the starting point for the calculation of matrix elements ((23) and (27)) The latter has been implemented into the *fhimd* code [57]. The main feature of the Si(100) surface reconstruction is the Si surface dimer. At low temperature, the most likely structure is the $c(4 \times 2)$ or $p(2 \times 2)$ reconstruction [5, 58]. As the numerical effort grows considerably with the size of the unit cell, we decided to use the simplest possible (2×1) surface unit cell for this preliminary study.

The calculation of the surface atomic structure is carried out using a regular 4×4 mesh to sample the Brillouin zone. The calculations are performed on an 8-layer slab. The surface geometry known from the literature [5, 58] (in particular the dimer tilt angle) are well reproduced. The calculation is performed using a plane-wave cutoff energy of 10 Ry, which corresponds to a total number of approximately 2300 plane waves (different $\boldsymbol{G}$-vectors in (4)) per $\underline{k}$-point.

In the next step, the band structure is calculated using the obtained optimized atomic structure. As the relaxation processes occur on excited states, a number conduction band states has to be included in the band structure calculation. In Fig. 6, the resulting band structure on a path of $\bar{\Gamma} - \bar{X} - \bar{M} - \bar{X}' - \bar{\Gamma}$ is given. The main difference to a bulk Silicon structure are the D_{up} and D_{down} surface states inside the bandgap. While the D_{up} band is mainly due to dangling bond orbitals at the upper Si atom, and is occupied by two-electrons, the D_{down} band stemming from the dangling orbitals of the lower Si atoms is unoccupied. Band structures for the more complex reconstructions can be found in the literature [59, 60].

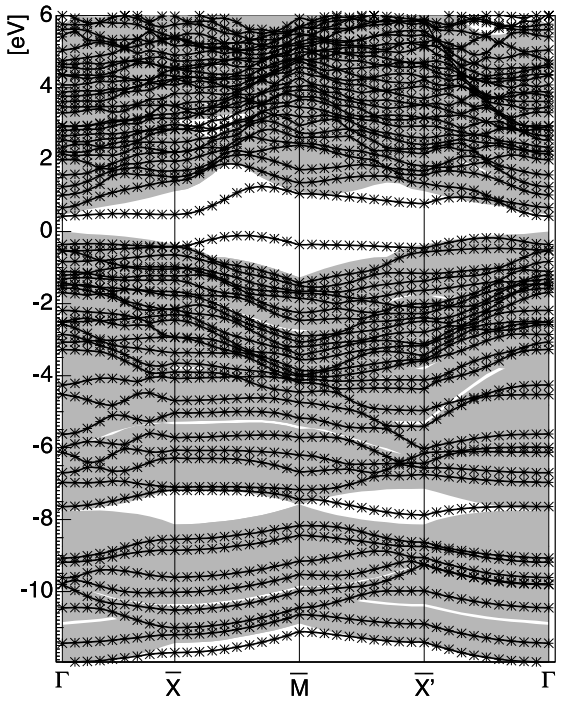

FIGURE 6 DFT-LDA band structure of Si(100). The energy range of the bulk bands is plotted in grey

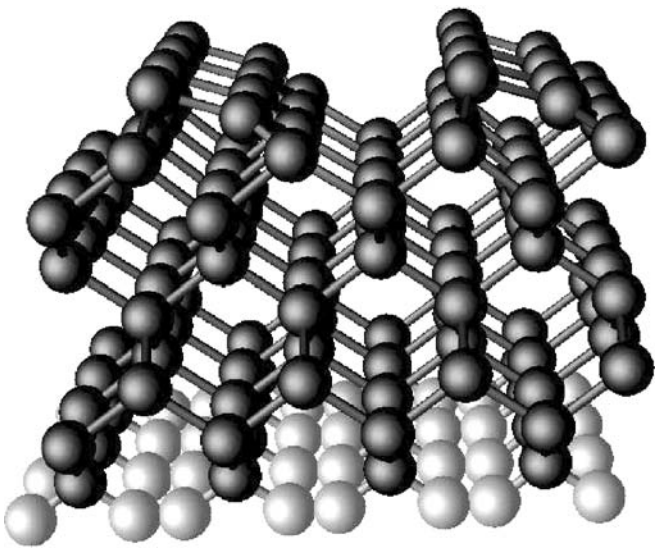

FIGURE 7 Ball-and-stick model of the Si(100) (2×1) 8-layer slab. On *top*, the buckled dimers can be observed. At the *bottom*, the structure is saturated by one layer of hydrogen atoms. For this picture, the elementary cell is repeated 2 times in k_x and 4 times in k_y direction

In Fig. 7, The (2x1) elementary cell after surface reconstruction is shown. On the top, one observes the buckled dimer at the surface. The optics and electron relaxation dynamics of these surface states (coupled to bulk states) are the main goal of the unified approach presented here.

5.2 *Matrix elements*

The calculation of matrix elements from the Kohn–Sham wave functions is straightforward; however, this step involves considerable computational effort: The dynamical evolution equations require the wave functions to be known on a finely discretized regular mesh of the Brillouin zone. Hence it is recommendable to parallelize the band structure calculation. The test calculations we performed so far indicate a discretization of 17×17 or higher is required for a converged dynamical evolution. The *fhimd* software being a plane wave code, the results of the Bloch wave functions are given in a form similar to (4), with the constraint that the number of reciprocal lattice vectors $\{\boldsymbol{G}\}$ is limited by the cutoff energy. The use of (23) for the phonon matrix elements and (27) for the optical dipole matrix elements is therefore a straightforward application.

At present, we work with bulk-projected phonon modes, as described in Sect. 2.1.2, without taking into account surface modes explicitly. Although this is a rather drastic assumption for the surface–surface scattering (there one would expect, due to the surface localization of the electron states, a strong coupling to surface modes), it is reasonable for the bulk–bulk an bulk–surface scattering, because the electronic bulk states are not likely to couple strongly to surface modes.

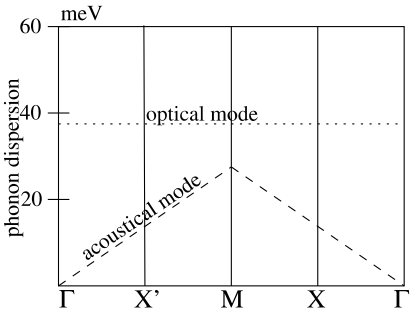

FIGURE 8 The effective phonon modes used in this work for Si(100). For a full set of phonon modes, see [62]

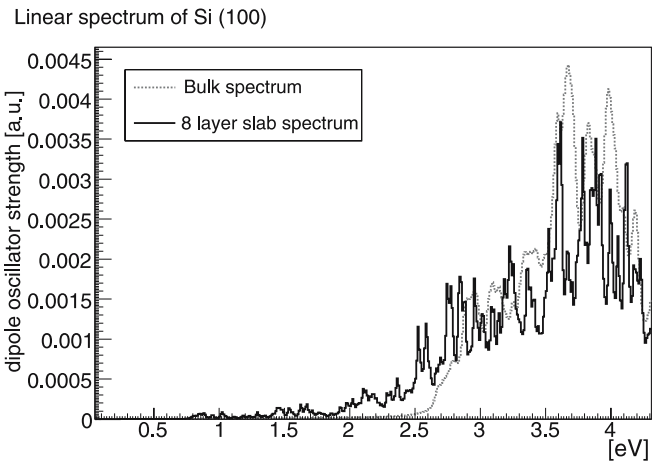

FIGURE 9 Linear spectra of an 8 layer slab (with surface reconstruction) and of a bulk system (without surface reconstruction)

So far, the phonon coupling strengths $D_{i\underline{q}}$ (see Sect. 3.1) are taken as constant experimental deformation potentials from bulk theory [43]. It is obvious that the surface–surface processes [61] have to be treated separately, and so far, the surface–surface matrix elements are taken to be a factor of three higher than the surface–bulk matrix elements to account for the strong coupling of the surface states to the dimer buckling mode. The phonon dispersion relations $\omega_{i\underline{q}}$ can be obtained by projecting the reciprocal bulk cell to the reciprocal slab cell (see Sect. 2.1.2). For this simulation, the phonon spectrum is treated schematically by the choice of two "effective" modes (Fig. 8): one optical mode approximately at the mean value of the whole phonon energy range and one acoustical mode with a linear dispersion at the bottom of the dispersion modes.

So far, real optical excitations have not been implemented in this simulation, but the calculation of optical matrix elements is numerically much less time-consuming than the phonon–electron matrix elements. In a separate investigation, we have done preliminary calculations of linear spectra (linear response to an external electrical field) from optical matrix elements (Fig. 9). There it is well observable that inside the band gap ($E < 2.5$ eV), new spectral lines appear which are due to the surface states of the Si(100) surface. It is clear that in this approach, exciton formation is neither considered in the DFT-LDA nor in the interactions treated in DMT. Hence it is not surprising that the bandgap width is so far incorrect and that excitonic peaks are absent from the spectrum.

5.3 *Numerical simulation – self-consistent solution of density matrix equations including ab-initio material constants*

The complete numerical simulation procedure involves four subsequent computational steps: first, the structure relaxation run to calculate the surface reconstruction and the electron density, second, the band structure run to calculate the energy dispersion and electron wave functions on a highly discretized regular mesh, third the calculation of the electron–phonon matrix elements and forth and last the dynamical simulation of the population evolution on the relevant bands. Most CPU time for the full simulation is required by the first step (40%) and the second step (40%). The band structure calculation (second step) is solved in parallel computing. The calculation of matrix elements (third step, 15%) and the dynamical evaluation up to a time step of 190 ps (forth step, 5%) are relatively fast. The requirement of system memory is limited mainly by the structure relaxation run (first step), while the code parallelization of the band structure calculation (second step) and the calculation of matrix elements (third step) allow a drastic reduction of memory consumption and the dynamical simulation (forth step) has only a minor need of computer memory. With the parameters of our simulation, the memory requirement is about 400 MB.

The consumption of disk space, however, is considerable. With the chosen run time parameters and discretization, about 1.5 GB for saving the wave function data in the first two steps are needed, the matrix elements (third step) require another 100 MB, while the space for saving of the dynamical population (forth step) is below 1 MB. These values are very sensitive to slab thickness and discretization in k-space.

As the investigated relaxation processes are restricted to a well defined energy range in the lower-lying conduction band region, it is reasonable to restrict the electron–phonon dynamics to a low number of bands. In the current implementation, as the main interest are the relaxation processes to and inside the surface state, we take the five lowest conduction bands besides the D^{down} state into account.

To focus on the relaxation phenomena, optical excitation is not treated explicitly so far, but by a reasonably chosen initial non-equilibrium electron distribution. Thus only the simplified set of dynamical equations (20) has to be used. The right-hand side of this systems of coupled differential equations can be evaluated efficiently by making use of matrix-vector and vector-vector operations, provided that the whole set of rates (labelled Γ in (20)) is calculated a priori by evaluating the δ-conditions inside these equations. This involves an inversion of the corresponding band structure

$$E_n(k_x, k_y) \rightarrow k_y(E_n, k_x) \tag{37}$$

and phonon dispersion functions

$$\omega_i(q_x, q_y) \rightarrow q_y(\omega_i, q_x)\,. \tag{38}$$

The ordinary differential equations can solved using a Runge–Kutta algorithm. The calculation is carried out on the $\underline{k}$-point mesh provided by the matrix element calculation on a picosecond timescale. We find that Runge–Kutta of order four is sufficient for most applications.

5.4 *Results for the electron cooling dynamics*

The focus in this section lies on the explanation of the equilibration of a non-equilibrium electron distribution due to its coupling to the bath of phonons at a fixed temperature $T = 300\,\mathrm{K}$. The phonons provide a large reservoir to cool the electrons to an equilibrium distribution via the electron–phonon interaction. To study the relaxation dynamics in realtime, an initial non-thermal population distribution is provided by hand in order to mimic the optical excitation of the system. It is reasonable to choose a set of initial conditions that approximates an optical excitation process. This is done by setting a Gaussian shaped distribution function around the energy corresponding to the supposed frequency of the excitation pulse. By this, the narrow range of an optical excitation is well modelled, while the dipole selection rules that could modulate the interband excitation probabilities within the energy range accessible by the excitation, are ignored. Their influence is left to future work. Due to this initial condition which shows no spatial inhomogeneity, all off diagonal elements of the density matrix are equal to zero (20).

For this primary simulation, we choose a rather high excitation energy of 2 eV above the surface band minimum at the $\bar{\Gamma}$ point with a width of 0.3 eV to get an overview of all the processes in this surface material system. In Fig. 10, the population of all electron states is plotted over the energy scale. Consequently, three types of relaxation are in the course of time: First only relaxation inside the bulk bands occurs, reflecting local features (band minima) of the band structure. After a certain time (ca. 40 ps), the bulk relaxation has reached states that are energetically sufficiently low ($\approx 0.5\,\mathrm{eV}$) to couple to the surface band. From this point on, electron scattering from the bulk to the surface band is more pronounced. Obviously, this is much slower than scattering inside the bulk, so an isolated peak at the local bulk band minimum (dashed line at 0.3 eV) is clearly visible (time = 50–120 ps). Once some population has entered the surface band, the scattering inside this band occurs on a rather fast time scale, and a Fermi-like distribution builds up on the low edge of the energy scale (time > 50 ps). Although some relaxation channels are obviously very fast, an equilibrium distribution is not achieved after a relaxation time of 190 ps. In particular, there are some electron states around the initial excitation point that appear to be very weakly coupled to any other state. One reason for this may be the restriction to only five bulk bands. Although the initial condition does not allow a clear extraction of the involved timescales for the relaxation, we find an scattering rate of approximately 150 ps for the bulk–surface scattering and of below 10 ps for the surface–surface scattering. This is a good agreement with the experimental data [14]. It should be mentioned that exciton formation is supposed to appear at the surface band minimum. This is, of course, not treated by our current calculation, since no Coulomb interaction has been taken into account in the dynamical equations [63].

On the rhs of Fig. 10, the population throughout the Brillouin zone is plotted. It can be seen that the population undergoes a shift through the zone. Initially, the populated states are found in the band structure between the $\bar{X}$ and $\bar{M}$ points, which is well reflected by the energy dispersion in the band structure. During relaxation, several local minima are populated, and finally, the surface band minimum at $\bar{\Gamma}$ gains importance. In thermal equilibrium, the whole population is located around $\bar{\Gamma}$.

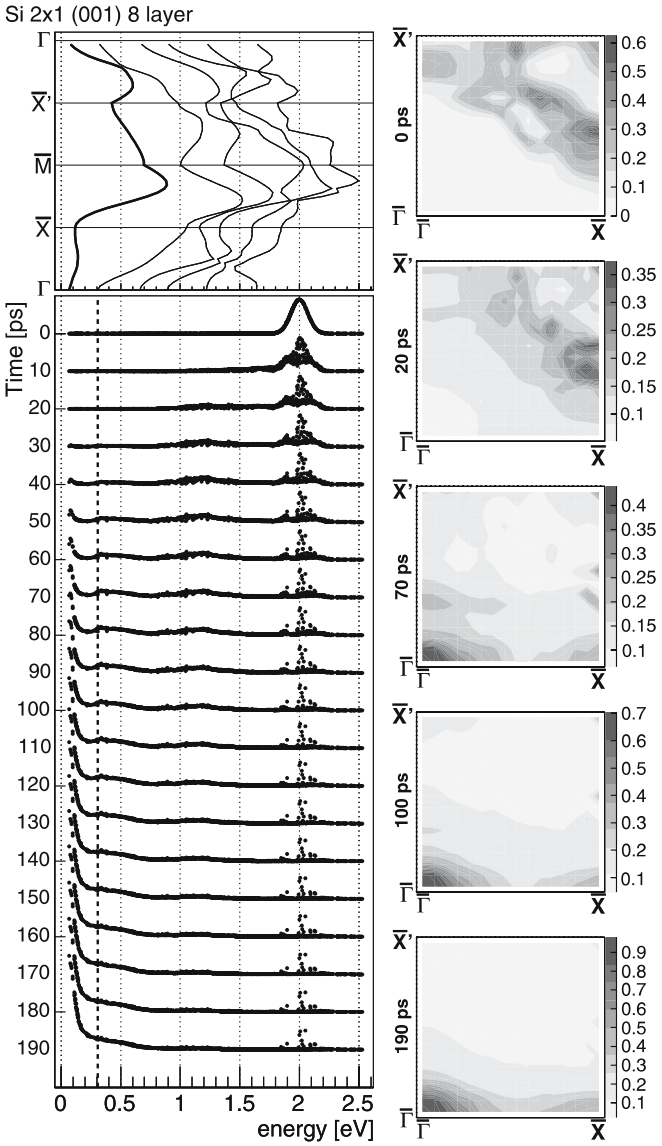

FIGURE 10 Relaxation simulation of the lower conduction band area of Si(100). On the *lhs*, at *top*, the band structure is depicted. The lowest band (*broad line*) on the *left* in the band structure is the D^{down}-surface band. An initial Gaussian distribution at 2 eV above the valence band maximum with a width of 0.3 eV is provided. The bulk conduction band minimum is indicated by the *dashed line* in the temporal evolution of the electron distribution (*bottom of lhs*). On the *rhs*, a top view of the Brillouin zone during relaxation is shown

6 Conclusion

In this paper, the feasibility of self-consistently combining density functional theory within LDA-approximation and density matrix theory to describe dynamical processes at semiconductor surfaces is demonstrated. In particular, the use of density functional theory to calculate interaction matrix elements produced very promising results in an detailed description of relaxation processes, for example the time-scales so far observed are in a good agreement with the

experimental data [14]. Nevertheless, some improvements of the method should be applied in order to address more realistic situations:

First, an explicit calculation of the phonon modes is required. Even though the use of two effective modes did not present an obvious failure of the model system, the local behaviour of relaxation could strongly depend on the phonon dispersion. Second, a higher number of layers should be used in the slab model. Although the surface properties start to converge at the slab thickness used here, a thicker slab leads to a higher number of bands and thus to a finer discretization of the energy scale. Finally, optical excitation as well as Coulomb interaction of the excited electron and holes [59, 63] should be included into the dynamical equations in order to allow a closer comparison to experimental data.

ACKNOWLEDGEMENTS We thank the Deutsche Forschungsgemeinschaft for support through Schwerpunktprogramm 1093. We thank A. Zeiser, F. Willig, L. Töben, L. Gundlach, P.H. Hahn, W.G. Schmidt and F. Bechstedt for useful discussions and collaboration.

REFERENCES

1 M. Lindberg, S.W. Koch, Phys. Rev. B **38**, 3342 (1988)
2 H. Haug, S.W. Koch, *Quantum Theory of the Optical and Electronic Properties of Semiconductors* (World Scientific, Singapore, 1990)
3 V.M. Axt, S. Mukamel, Rev. Mod. Phys. **70**, 145 (1998)
4 F. Rossi, T. Kuhn, Rev. Mod. Phys. **74**, 895 (2002)
5 J. Dabrowski, M. Scheffler, Appl. Surf. Sci. **56**, 15 (1992)
6 M. Reichelt, T. Meier, S.W. Koch, M. Rohlfing, Phys. Rev. B **68**, 045 330 (2003)
7 E. Knoesel, A. Hotzel, M. Wolf, Phys. Rev. B **57**, 12 812 (1998)
8 U. Höfer, I.L. Shumay, C. Reuß, U. Thomann, W. Wallauer, T. Fauster, Science **277**, 1480 (1997)
9 C. Gahl, K. Ishioka, Q. Zhong, A. Hotzel, M. Wolf, Faraday Discuss. **117**, 191 (2000)
10 Q. Zhong, C. Gahl, M. Wolf, Surf. Sci. **496**, 21 (2002)
11 C.A. Schmuttenmaer, C.C. Miller, J.W. Herman, J. Cao, D.A. Mantell, Y. Gao, R.J.D. Miller, Chem. Phys. **205**, 91 (1996)
12 V.P. Zhukov, O. Andreyev, D. Hoffman, M. Bauer, M. Aeschlimann, E.V. Chulkov, P.M. Echenique, Phys. Rev. B **70**, 233 106 (2004)
13 L. Töben, L. Gundlach, R. Ernstorfer, R. Eichberger, T. Hannappel, F. Willig, A. Zeiser, J. Förstner, A. Knorr, P.H. Hahn, W.G. Schmidt, Phys. Rev. Lett. **94**, 067 601 (2005)
14 M. Weinelt, M. Kutschera, T. Fauster, M. Rohlfing, Phys. Rev. Lett. **92**, 126 801 (2004)
15 M. Bonn, D.N. Denzler, S. Funk, M. Wolf, S.-S. Wellershoff, J. Hohlfeld, Phys. Rev. B **61**, 1101 (2000)
16 R. Haight, Surf. Sci. Rep. **21**, 275 (1995)
17 A. Rettenberger, R. Haight, Phys. Rev. Lett. **76**, 1912 (1996)
18 T. Hertel, E. Knoesel, M. Wolf, G. Ertl, Phys. Rev. Lett. **76**, 535 (1996)
19 T. Klamroth, P. Saalfrank, U. Höfer, Phys. Rev. B **64**, 35 420 (2001)
20 S. Ramakrishna, F. Willig, A. Knorr, Appl. Phys. A **78**, 247 (2004)
21 S. Ramakrishna, F. Willig, A. Knorr, Surf. Sci. **558**, 159 (2004)
22 A. Zeiser, N. Bücking, J. Götte, J. Förstner, P. Hahn, W. Schmidt, A. Knorr, Phys. Stat. Solidi B **241**, R60 (2004)
23 A. Zeiser, N. Bücking, J. Förstner, A. Knorr, Phys. Rev. B **71**, 245 309 (2005)
24 G. Onida, L. Reining, A. Rubio, Rev. Mod. Phys. **74**, 601 (2002)
25 M.C. Desjonquères, D. Spanjaard, *Concepts in Surface Physics* (Springer, Berlin, 1996)
26 F. Bechstedt, R. Enderlein, *Semiconductor Surfaces and Interfaces* (Akademie-Verlag, Berlin, 1988)
27 G. Czycholl, *Theoretische Festkörperphysik* (Vieweg, Braunschweig/Wiesbaden, 2000)
28 F. Bechstedt, *Principles of Surface Science* (Springer, Berlin, 2003)
29 N.W. Ashcroft, N.D. Mermin, *Solid State Physics* (Holt-Saunders International Editions, Tokyo, 1981)
30 H. Lüth, *Surfaces and Interfaces of Solids* (Springer, Berlin, 1993)
31 H. Haken, *Quantenfeldtheorie des Festkörpers* (B.G. Teubner, Stuttgart, 1973)
32 J.D. Jackson, *Classical Electrodynamics* (John Wiley & Sons Inc., New York, 1999)
33 H. Haug, A.P. Jauho, *Quantum Kinetics in Transport and Optics of Semiconductors*, in: *Springer Series in Solid-State Sciences*, vol. 123 (Springer, Berlin, 1998)
34 T. Kuhn. *Density matrix theory of coherent ultrafast dynamics*, in: *Theory of Transport Properties of Semiconductor Nanostructures*, ed. by E. Schöll (Chapman & Hall, London, 1998), p. 173
35 V.M. Axt, A. Stahl, Z. Phys. B **93**, 195 (1994)
36 M. Lindberg, R. Binder, Y.Z. Hu, S.W. Koch, Phys. Rev. B **49**, 16 942 (1994)
37 J. Fricke, Ann. Phys. **252**, 479 (1996)
38 I. Waldmüller, J. Förstner, S.-C. Lee, A. Knorr, M. Woerner, K. Reimann, R.A. Kaindl, T. Elsaesser, R. Hey, K.H. Ploog, Phys. Rev. B **69**, 205 307 (2004)
39 T. Feldtmann, L. Schneebeli, M. Kira, S.W. Koch, Phys. Rev. B **73**, 155 319 (2006)
40 J. Förstner, C. Weber, J. Danckwerts, A. Knorr, Phys. Rev. Lett. **91**, 127 401 (2003)
41 I. Waldmüller, J. Förstner, S.C. Lee, A. Knorr, M. Woerner, K. Reimann, R.A. Kaindl, T. Elsaesser, R. Hey, K.H. Ploog, Phys. Rev. B **69**, 205 307 (2004)
42 W. Schäfer, M. Wegener, *Semiconductor Optics and Transport Phenomena* (Springer, Berlin, 2002)
43 P.Y. Yu, M. Cardona, *Fundamentals of Semiconductors* (Springer, Berlin, 1996)
44 W. Pötz, P. Vogl, Phys. Rev. B **24**, 2025 (1981)
45 C.G. van der Walle, Phys. Rev. B **39**, 1871 (1989)
46 R. DelSole, R. Girlanda, Phys. Rev. B **48**, 11 789 (1993)
47 F. Steininger, A. Knorr, T. Stroucken, P. Thomas, S.W. Koch, Phys. Rev. Lett. **77**, 550 (1996)
48 I. Waldmüller, J. Förstner, A. Knorr, *Nonequilibrium Physics at Short Time Scales*, Chapt. *Self-consistent Projector Operator Theory of Intersubband Absorbance in Semiconductor Quantum Wells* (Springer, Berlin, 2003)
49 P. Hohenberg, W. Kohn, Phys. Rev. B **136**, 864 (1964)
50 W. Kohn, L.J. Sham, Phys. Rev. A **140**, 1133 (1965)
51 R. Haight, J. Bokor, J. Stark, R.H. Storz, R.R. Freeman, P.H. Bucksbaum, Phys. Rev. Lett. **54**, 1302 (1985)
52 W.G. Schmidt, F. Bechstedt, Surf. Sci. **409**, 474 (1998)
53 W.G. Schmidt, F. Bechstedt, N. Esser, M. Pristovsek, C. Schultz, W. Richter, Phys. Rev. B **57**, 14 596 (1998)
54 A.M. Frisch, P. Vogt, S. Visbeck, T. Hannappel, F. Willig, W. Braun, W. Richter, J. Bernholc, W.G. Schmidt, N. Esser, Appl. Surf. Sci. **166**, 224 (2000)
55 W.G. Schmidt, N. Esser, A.M. Frisch, P. Vogt, J. Bernholc, F. Bechstedt, M. Zorn, T. Hannappel, S. Visbeck, F. Willig, W. Richter, Phys. Rev. B **61**, R16 335, (2000)
56 L. Töben, L. Gundlach, T. Hannappel, R. Ernstorfer, R. Eichberger, F. Willig, Appl. Phys. A **78**, 239 (2004)
57 M. Bockstedte, A. Kley, J. Neugebauer, M. Scheffler, Comput. Phys. Commun. **107**, 187 (1997)
58 A. Ramstad, G. Brocks, P.J. Kelly, Phys. Rev. B **51**, 14 504 (1995)
59 M. Rohlfing, S.G. Louie, Phys. Rev. Lett. **83**, 856 (1999)
60 P. Eggert, *Theoretische Untersuchung von Vielteilcheneffekten auf Silizium-Halbleiteroberflächen*, PhD thesis, FU Berlin (2005)
61 J. van Heys, M. Lindenblatt, E. Pehlke, Phase Trans. **78**, 773 (2005)
62 J. Fritsch, P. Pavone, Surf. Sci. **344**, 195 (1995)
63 W. Hoyer, M. Kira, S.W. Koch, Phys. Rev. B **67**, 155 113 (2003)